Cooperative Ordering and Kinetics of Cellulose Nanocrystal Alignment in a Magnetic Field

Kevin J. De France, Kevin G. Yager, Todd Hoare, and Emily D. Cranston

DOI: **10.1021/acs.langmuir.6b01827**

Cooperative Ordering and Kinetics of Cellulose Nanocrystal Alignment in a Magnetic Field

Kevin J. De France[1], *Kevin G. Yager*[2], *Todd Hoare*[1], *Emily D. Cranston*[1]*

1. Department of Chemical Engineering, McMaster University, 1280 Main Street West, Hamilton, ON L8S 4L8, Canada
2. Center for Functional Nanomaterials, Brookhaven National Laboratory, Upton, NY, USA

Keywords: cellulose nanocrystals, magnetic alignment, small angle x-ray scattering, chiral nematic liquid crystal, cooperative ordering

Abstract

Cellulose nanocrystals (CNCs) are emerging nanomaterials which form chiral nematic liquid crystals above a critical concentration (C^*) and additionally orient within electromagnetic fields. The control over CNC alignment is significant for material processing and end-use; to date, magnetic alignment has only been demonstrated using strong fields over extended or arbitrary timescales. This work investigates the effects of comparatively weak magnetic fields (0 – 1.2 T) and CNC concentration (1.65 – 8.25 wt%) on the kinetics and degree of CNC ordering using small angle x-ray scattering. Interparticle spacing, correlation length, and orientation order parameters (η and S) increased with time and field strength following a sigmoidal profile. In a 1.2 T magnetic field for CNC suspensions above C^*, partial alignment occurred in under 2 min followed by slower cooperative ordering to achieve near-perfect alignment in under 200 min (S = –0.499 where S = –0.5 indicates perfect anti-alignment). At 0.56 T, near-perfect alignment was also achieved, yet the ordering was 36% slower. Outside of a magnetic field, the order parameter plateaued at 52% alignment (S = –0.26) after 5 hours, showcasing the drastic effects of relatively weak magnetic fields on CNC alignment. For suspensions below C^*, no magnetic alignment was detected.

Introduction

In the past decade, cellulose nanocrystals (CNCs) have gained attention due to the vast abundance of renewable cellulosic source materials, their impressive physicochemical properties, and their recent large scale commercial production.[1–3] In most cases, CNCs are prepared by sulfuric acid-mediated hydrolysis of wood pulp or plant fibers, yielding rod-like crystalline nanoparticles that are colloidally stable in water due to anionic sulfate half-ester surface groups.[4,5] Above a critical concentration (C^*), CNC suspensions spontaneously phase separate into a biphasic regime (cf. Onsager translational entropy gain[6]) containing an upper isotropic phase and a lower anisotropic chiral nematic liquid crystalline phase.[5,7] The critical concentration and phase behavior are largely dependent on the CNC aspect ratio, surface chemistry, and ionic strength of the suspension.[8]

Many high-performance natural biocomposites (e.g. lobster cuticle and beetle shells) result from liquid crystalline self-assembly;[8] as a result, controlling alignment and self-assembly is of interest for developing mechanically strong biomimetic materials.[9] Furthermore, chiral nematic thin films are iridescent and selectively reflect light, which may be useful for optical filters, sensors and decorative coatings.[10] CNC films with controlled optical properties and structural color have been demonstrated in both CNC-only materials[11] and CNCs combined with water-soluble polymers to improve flexibility;[12,13] however, uniform long-range order can be challenging to achieve. Work pioneered by the Maclachlan group has moreover used CNCs to template other materials to obtain chiral nematic porous structures, including silica, carbon, germania, polymer resins, and hydrogels.[10,14,15] Furthermore, unidirectional freezing of CNC dispersions has been shown to produce foams with aligned CNCs and anisotropic pores.[16] Similarly, tissue engineering scaffolds containing oriented CNCs may offer templating

possibilities and guidance for directional cell growth and orientation-induced differentiation;[17,18] however, applications such as these require near-perfect orientation. As such, having a straightforward and reproducible way to manipulate CNC alignment is crucial for further development of functional materials.

Within an individual cellulose nanocrystal, there is a high degree of molecular orientation and as such, external electromagnetic fields can encourage both linear and chiral nematic alignment.[19] Electric field alignment, while effective, requires CNCs to be suspended in non-polar solvents to avoid complications arising from the high conductivity of water.[20–22] Given that CNCs are not colloidally stable in such media, coupled with the fact that organic solvents are discouraged in industrial processing, magnetic alignment may offer a more feasible route to produce controllably aligned CNC materials.[23–25]

Sugiyama *et al.* were the first to show that the magnetic dipole of individual C–O, C–H, and O–H bonds, and their relative orientations in the cellulose polymer chain, led to a material with anisotropic diamagnetic susceptibility.[26] Furthermore, it was observed that the diamagnetic susceptibility is smaller in the direction parallel to the polymer chain axis compared to the perpendicular direction, characterizing cellulose more specifically as a *negative* diamagnetic anisotropic material.[24] Recently, this diamagnetic susceptibility has been calculated for dilute suspensions of CNCs (-0.95×10^{-6}), a value that agrees well with estimations from Pascal's additivity law.[27]

Due to the liquid crystalline properties of CNC suspensions, the response in a magnetic field differs above and below the critical concentration. Below C^*, given a strong enough field, CNCs should orient linearly perpendicular to the magnetic field to give long range uniaxial

(nematic) order.[26] Above *C**, the anisotropic phase contains CNCs arranged in chiral nematic tactoids (small local regions with order).[28] Given time, the tactoids grow larger and merge together, increasing the degree of long range order in the liquid crystal.[29] In a magnetic field, the chiral nematic tactoids are preferentially reoriented with the helical chiral nematic director parallel to the magnetic field, again leading to orientation of CNCs perpendicular to the field.[24] Such orientation leads to a uniform chiral nematic texture across the entire anisotropic fraction of the liquid, as demonstrated previously by circular dichroism and neutron scattering experiments.[28,30,31] The chiral nematic pitch (*P*), which describes the interparticle spacing and the resulting optical properties is defined as one full twist of the chiral nematic structure, and can be changed in a predictable manner by varying the ionic strength, CNC surface charge, or imposed magnetic field strength of a CNC suspension, providing a versatile way to control material performance.[32]

Although magnetic alignment of CNCs in suspension has been demonstrated in the literature, the fundamental kinetics of alignment and the required field strengths remain largely unknown. Previously, strong magnetic fields (as high as 28 T[33]) have been employed (sometimes for over 17 h[30,33,34]) in order to create highly aligned suspensions or dried films of CNCs.[23,24,26–28,30–38] Furthermore, past work has largely focused on the ordering of CNCs derived from tunicate (a marine invertebrate animal), which have a significantly higher aspect ratio than the CNCs produced commercially from wood pulp or the cotton source used herein.[39] As such, for the practical application of magnetic fields to obtain oriented CNC suspensions, a detailed understanding of the ordering of these anisotropic nanoparticles and the effects of field strength on alignment kinetics is crucial. In this work, we aim to address this gap in knowledge by studying the effects of CNC suspension concentration and magnetic field strength on the rate and

degree of CNC alignment via *in situ* small angle x-ray scattering (SAXS). Overall we find that very fast initial alignment is achievable for cotton-derived CNC suspensions above *C**, followed by slower cooperative alignment, even within relatively weak magnetic fields.

Experimental Section

Preparation and characterization of cellulose nanocrystal (CNC) suspensions.

CNCs were produced by sulfuric acid-mediated hydrolysis of cotton ashless filter aid (GE Healthcare Canada, CAT No. 1703-050).[39] Briefly, 40 g of filter aid was suspended in 700 mL of 64 wt% sulfuric acid (Sigma Aldrich, 95-98%) at 45 °C for 45 min and subsequently quenched with purified water (Millipore Milli-Q grade distilled deionized water with 18.2 MΩ cm resistivity). The suspensions were centrifuged at 6000 rpm for 10 min repeatedly with water, decanted, and replenished until a pellet no longer formed. The resulting CNC suspension was dialyzed (molecular weight cut-off = 12-14 kDa) against purified water for a minimum of ten cycles of at least 12 h per cycle until the pH of the suspension no longer changed. The CNC suspension was sonicated over an ice bath using a probe sonicator (Sonifier 450, Branson Ultrasonics, Danbury, CT) for three cycles of 15 minutes each and stored as a 1 wt% suspension in its acid form (pH = 3.2). Suspensions were concentrated to 1.65, 4.13 and 8.25 wt% by evaporation at ambient conditions, using gravimetry to determine final concentrations. All CNCs suspensions studied were in the acid-form, i.e., the sulfate half ester counterion was a proton, in contrast to many literature reports and commercially available CNCs which are neutralized to their sodium-form.

The sulfate half-ester content on the surface of the CNCs was determined via conductometric titration (100 mg of CNC in 100 mL of 10 mM NaCl as the analysis sample and

2 mM NaOH as the titrant),[40] yielding a sulfur content of 0.42 wt% (0.30 charges per nm^2). The electrophoretic mobility was -1.86×10^{-8} m^2 V^{-1} s^{-1} (measured for 0.25 wt% CNC suspensions in 10 mM NaCl using a ZetaPlus analyzer, Brookhaven Instruments Corp.). Atomic force microscopy (MFP-3D, Asylum Research and Oxford Instruments Company, Santa Barbara, CA) was used in alternating current mode with rectangular FMR cantilevers (NanoWorld) of normal spring constants 1.2–5.5 N/m to determine the average dimensions of CNCs. Open CNC films on piranha-cleaned silicon wafers were prepared by spin coating, and CNC dimensions of 8 ± 3 nm in cross section and 122 ± 47 nm in length were calculated based on ImageJ analysis of 80+ individualized nanocrystals in the AFM height image (error intervals are one standard deviation). These CNC dimensions were used in subsequent SAXS modeling assuming a cylindrical geometry. Furthermore, the properties of our CNCs are very similar to the work of Beck-Candanedo *et al.*[39] with acid-form CNCs extracted from black spruce wood pulp having dimensions of 147 ± 65 nm by 5 ± 0.4 nm with 0.33 charges per nm^2 and a C^* of 4.8 wt%. As such, the CNC suspensions studied here are considered well below (1.65 wt%), slightly below (4.13 wt%), and above (8.25 wt%) the critical concentration required for liquid crystalline phase separation. This was confirmed with polarized optical microscopy (Supporting Information, Figure S1), showing the presence of chiral nematic tactoids in 8.25 wt% suspensions only.

Small angle x-ray scattering (SAXS).

Small-angle x-ray scattering (SAXS) experiments were performed on a Bruker Nanostar instrument with a Cu K-α rotating anode source emitting 8.04 keV x-rays (wavelength $\lambda = 4.0784$ $Å^{-1}$). A two-pinhole (scatterless) collimation scheme was used, with the SAXS area detector positioned at 1.150 m from the sample; this configuration results in *q*-resolution of approximately 0.001 $Å^{-1}$. A typical accumulation time was 60 s, resulting in ~500,000 total

counts across the area detector (2048 × 2048 pixels). The data was standardized against the scattering spectrum obtained from a silver behenate sample utilizing computer software to convert data to reciprocal-space (q).

For *in situ* magnetic field experiments, a customized sample cell was used. Two permanent magnets (NdFeB, 1 inch diameter and 1 inch in length) were affixed to a track that enabled adjustable spacing between the magnets. At minimum separation (2 mm), the magnets generated a 1.2 T total field in the gap center, as estimated from manufacturer-provided calibration data (as a function of magnet separation distance), which were calculated based on measurements of the surface field, combined with finite element analysis (FEA) to compute the expected field within the gap. By increasing the gap width, the field strength could effectively be reduced. The samples were held in thin quartz capillaries (1 mm outer diameter, 100 μm wall thickness), that were inserted into the center of the magnetic gap, along the central axis of the cylinder-shaped magnets (in the x-direction, Figure 1b) where the magnetic field is the strongest and most uniform, minimizing error in field strength estimations. The x-ray beam was aligned vertically through the center of gap (in the z-direction). 0 T control experiments were performed with the magnets removed so as to determine any inherent alignment of the CNC suspensions.

For alignment kinetic experiments, the samples were loaded into the capillaries using a large-bore syringe to fill from the bottom of the capillary. Capillaries were sealed with wax to avoid evaporation due to the vacuum environment in the instrument sample chamber, and immediately inserted into the *in situ* cell (with or without an applied magnetic field) within the SAXS instrument. This preparation process took 2 minutes, at which time data acquisition was

initiated; note that some delay is unavoidable due to the pump-down time for the sample chamber. Times are reported with respect to the moment the sample was inserted into the magnetic field.

Two dimensional SAXS data was quantified in two main ways (η and S parameters); the $I(\chi)$ curve was fit phenomenologically to yield an ad-hoc order parameter (η) by fitting the curve to:[41–43]

$$I(\chi) = C\frac{1-\eta^2}{(1+\eta)^2 - 4\eta\cos^2(\chi-\chi_0)} \qquad \text{(Equation 1)}$$

where χ_0 is the alignment direction, and C is a scaling constant, with η varying from 0 (isotropic) to 1 (fully anisotropic). Furthermore, an assessment of the orientation of the CNCs themselves, where the average occurs over the orientations of all entities with respect to the desired director (χ) was performed. With knowledge of the orientation distribution ($f(\chi)$), the order parameter (S) is computed as:[44]

$$S = \frac{\int_0^{\pi/2} f(\chi')\frac{3\cos^2\chi'-1}{2}\sin\chi' d\chi'}{\int_0^{\pi/2} f(\chi')\sin\chi' d\chi'} \qquad \text{(Equation 2)}$$

where the substitution $\chi' = \pi/2 - \chi$ occurs because we define χ with respect to q_z (whereas χ' is defined with respect to the q_x axis). Under this definition, $S = 0$ indicates a random orientation distribution (isotropic), $S = 1$ indicates perfect alignment of all entities with respect to the director, and $0 < S < 1$ indicates intermediate levels of alignment. This definition also yields $S = -1/2$ for perfect anti-alignment, in which all entities are perpendicular to the director but there is orientational freedom within the plane orthogonal to the director. Values of S between 0

and –1/2 indicate varying amounts of (anti) alignment. It is important to note that SAXS does not differentiate between nematic and chiral nematic orientation and can only detect anisotropy in the beam direction; this means that although tactoids contain local order unless the CNCs themselves are preferentially aligned in the *yz* direction their orientation is undetected. Additionally, in our case (and in contrast to some liquid crystal literature) an *S* value of zero does not mean no chiral nematic ordering but merely that order is not aligned globally in the *yz* direction. Plotted error bars and error intervals reported are calculated from the standard error of regression.

To track the kinetic changes in CNC structuring as a function of time both inside and outside the magnetic field, we have fit the time evolution of the scattering parameters measured (based on fits to Equation 1 and Supporting Information Equation S1) to a phenomenological sigmoidal equation:

$$I(t) = I_i + (I_f + I_i)\frac{1}{1+\exp[-(t-\tau_1)/\tau_2]} \qquad \text{(Equation 3)}$$

Where τ_1 can be thought of as an "induction time" (i.e. the time for the auto-catalytic/ cooperative-ordering effects to arise) and τ_2 is the speed of the cooperative ordering itself; that is, it denotes how rapidly the system reaches the final (ordered, aligned) state once cooperative ordering begins. We characterize the overall timescale of the process as $\tau = \tau_1 + \tau_2$ (which corresponds to when the evolution is 73% complete). This shape is suggestive of a cooperative ordering process in which organization accelerates as more material is well-ordered and seeds further assembly until a maximum ordering is eventually achieved. Further SAXS theory and data analysis pertaining to CNC suspensions is presented in the Supporting Information.

Polarized optical microscopy (POM).

Optical micrographs were taken using a Nikon Eclipse LV100POL microscope. Digital images were taken between crossed polarizers at 10 times magnification of the bottom section of CNC suspensions sealed within flat capillary tubes (width = 10.0 mm, inner diameter = 1.0 mm).

Results and Discussion

We investigated the alignment of cotton-derived CNCs in a magnetic field, and extracted quantitative order parameters from *in situ* SAXS measurements. Figure 1 depicts the experimental setup, the liquid crystalline organization that CNCs adopt in suspension at concentrations above C^*, and the expected CNC orientation in a magnetic field. As a control, the anisotropy of CNC suspensions outside of a magnetic field was investigated. Figure 2 shows one-dimensional SAXS data for CNC suspensions at concentrations of 1.65, 4.13 and 8.25 wt%. Our CNCs have a C^* between 4.13 and 5.5 wt%, as determined through polarized optical microscopy (Supporting Information, Figure S1), which agrees strongly with the work of Beck-Candanedo *et al.*, who determined a C^* of 4.8 wt% for CNCs with similar properties,[39] such that chiral nematic orientation is only observed in the 8.25 wt% sample; all other concentrations tested (1.65 and 4.13 wt%) lie below C^*. At high concentrations, we observe a distinct $S(q)$ peak at low q (denoted q_0 in Figure 2), indicative of ordering, as described in the Supporting Information. The appearance of this peak is consistent with the literature[45,46] and can be ascribed to the local particle-particle packing distance between nematic "pseudo planes" of CNCs, $d_0 = 2\pi/q_0$ (where the term "pseudo" is used in recognition of the fact that the sample remains a free flowing liquid).

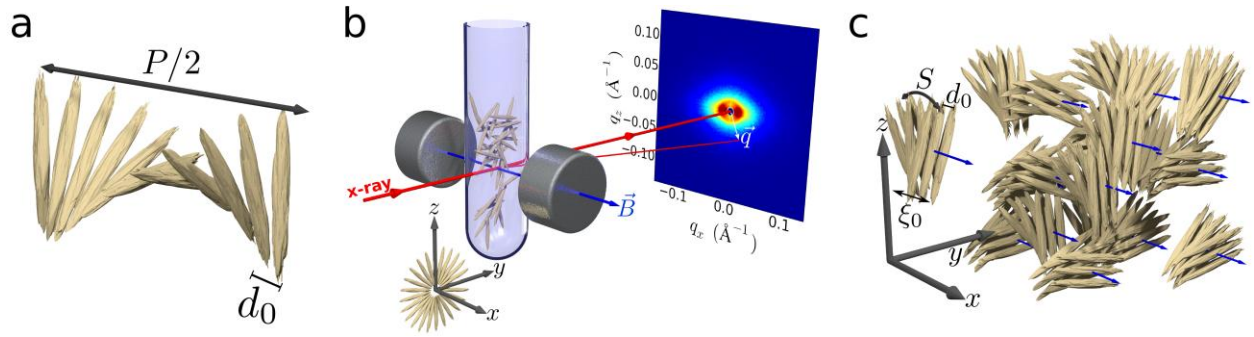

Figure 1. (a) Schematic of the chiral nematic liquid crystalline texture which CNCs adopt in suspension above *C**; one-half pitch (*P*) is depicted. (b) Experimentally, CNC suspensions were loaded into a capillary centered between permanent magnets. The x-ray beam (red) probes orthogonal to the magnetic field direction (blue, along the *x*-axis). Anisotropic scattering is collected on an area detector. CNCs orient perpendicular to the magnetic field direction (degenerate orientations shown at bottom). (c) CNCs pack and align with neighbors into tactoids. Because of the anti-alignment of CNCs with respect to the field (blue), ordered CNC tactoids are also anti-aligned. Ordering can be characterized by the packing distance (d_0), correlation length (ξ_0), and orientation order parameter (S).

The structural order peak in Figure 2 shifts to lower q for more dilute suspensions (i.e. lower CNC volume fractions), indicating larger inter-particle distances (d_0 = 37.8 ± 0.1 nm at 8.25 wt% and 45.4 ± 0.2 nm at 4.13 wt%). This result is consistent with observations by Schütz *et al*. on CNCs from wood pulp, which showed separation distances increasing from 25 nm at 10.4 wt% to 51 nm at 2.1 wt%.[46] At the lowest CNC concentration tested (1.65 wt%), the *S(q)* peak is broad, indicative of weakly-ordered packing due to the low volume fraction of nanoparticles in suspension;[34,46] as such, separation distances could not be accurately calculated.

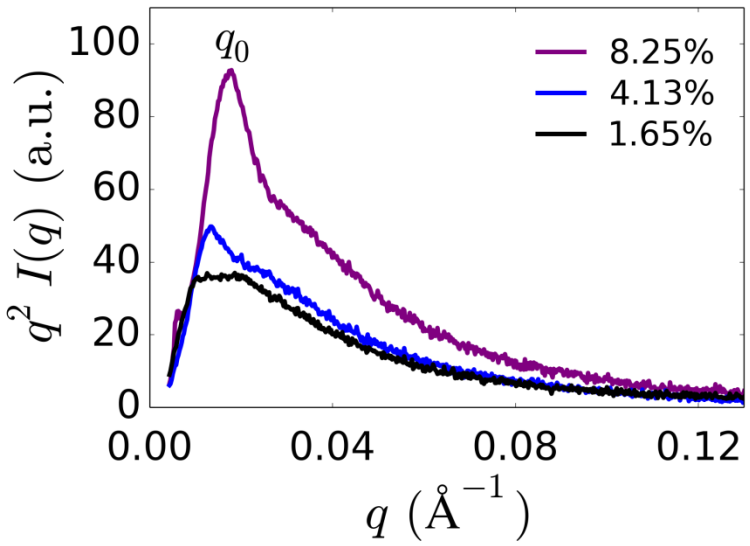

Figure 2. One-dimensional circularly averaged scattering intensity for CNC suspensions at varying concentration, outside of a magnetic field. Data is multiplied by q^2 (Kratky-plot) to emphasize the structural features. At high CNC concentration, a distinct structural peak (labeled q_0) appears for the 4.13 and 8.25 wt% CNC curves.

The anisotropy of CNC suspensions in a magnetic field was assessed by extracting the x-ray scattering intensity along an arc of constant q (where the angular direction about the beam is denoted by χ). Figure 3 compares suspensions below and above C^* after exposure to a 1.2 T magnetic field for 5 hours. For the lower concentration CNC suspensions, 4.13 wt% (Figure 3a) and 1.65 wt% (Figure S2, Supporting Information), the scattering patterns are essentially isotropic, implying minimal orientation of CNCs under the field conditions employed. Conversely, the anisotropy of the higher concentration CNC suspension (Figure 3b) is evident in the 2D scattering and highlighted in the $I(\chi)$ data. The peaks at χ = –90º and +90° observed for the 8.25 wt% CNC suspension arise due to scattering from CNC packing along the short axis (cross section) direction, and indicate a high degree of order perpendicular to the applied magnetic field.

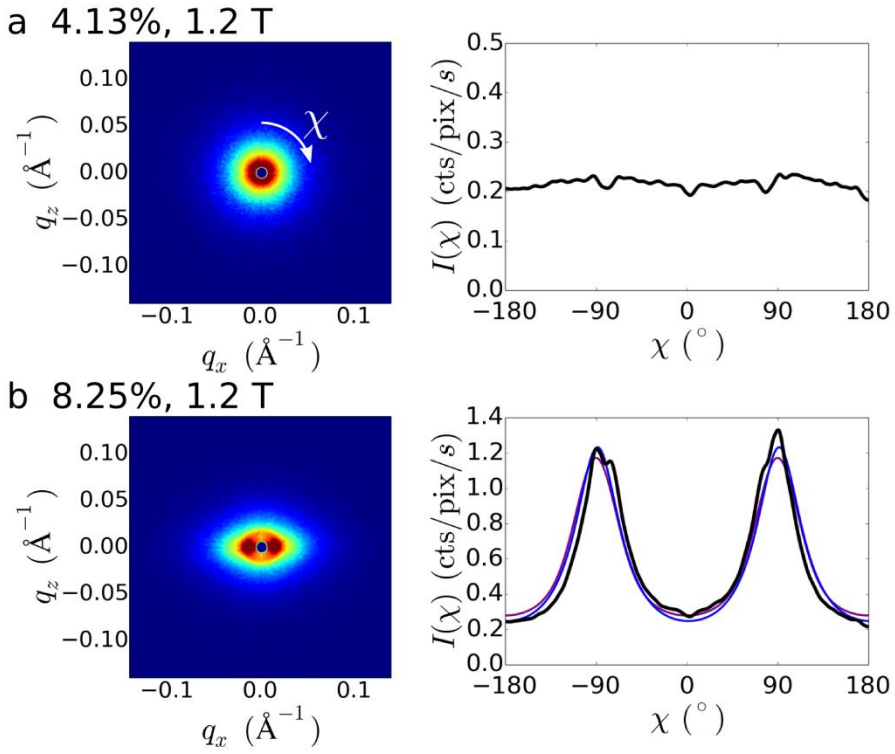

Figure 3. Two-dimensional scattering intensity for two representative CNC suspensions after ordering within a magnetic field (1.2 T): (a) 4.13 wt% is below *C** and (b) 8.25 wt% is above *C**. On the right, the corresponding intensity at constant q_0 = 0.017 Å^{-1} as a function of angle (χ) is shown in units of counts per pixel per second. Fits of the experimental data (black) are provided to an ad-hoc orientation function (blue, Equation 1) and to the Maier-Saupe distribution (purple, Equation S1-Supporting Information) and the choice of model and associated errors are discussed further in the Supporting Information.

The development of CNC ordering over time was investigated by taking sequential SAXS measurements every minute on CNC suspensions placed inside the magnetic field. Figure 4 shows the development of the intensity peaks, inter-particle spacing, correlation length, and orientational order over 250 min for the 8.25 wt% CNC suspension ($C > C^*$). By fitting time-lapsed data similar to that shown in Figure 3 with two different methods (described in the Supporting Information), orientation order parameters η and S were calculated. The first order parameter, η comes from a phenomenological fit to Equation 1, with $\eta \rightarrow 1$ for perfectly aligned materials. On the other hand, S is related to the typical orientation order parameter used to describe liquid crystals where $S = -1/2$ represents perfect anti-alignment (expected for CNCs in a

magnetic field). S is calculated from the SAXS data according to Equation 2, with the subscripts i and f representing initial and final order parameters respectively. The use of different scattering functions $I(\chi)$ to calculate S and the associated error is discussed further in the Supporting Information.

The observed trends in Figure 4 are ultimately related to the alignment of the CNCs perpendicular to the applied magnetic field. There is a shift and narrowing of the structural q_0 peak and an increase in scattering intensity over time, indicative of improved order (a larger fraction of CNCs packing in a well-defined manner). The corresponding particle packing distance d_0 increases, albeit less than 1 nm total, as ordering proceeds, indicative of the expected increase in local "free volume" as CNC suspensions transition from disordered to ordered and CNCs co-align with neighbors in nematic pseudo planes. Additionally, as tactoids grow the number of dislocations is reduced which will also contribute to a larger average spacing between particles. (The term "free volume" is used to indicate volume that could be occupied by CNCs[47] - this volume increases as rods co-align, as described by Onsager[6].)

The correlation length (Scherrer coherence length) of CNC packing (ξ_0, derived from the width of the primary structural peak as described in the Supporting Information) increases with time, implying a more well-defined assembly. Note that correlation lengths in this range mean that there are only a small number of CNC particles in each packing repeat ($\xi_0 < 2d_0$), which would normally imply rather poor ordering; however, the chiral nematic structure of CNC ordering means that the particle-particle scattering necessarily decorrelates over distances equal to the chiral nematic pitch.

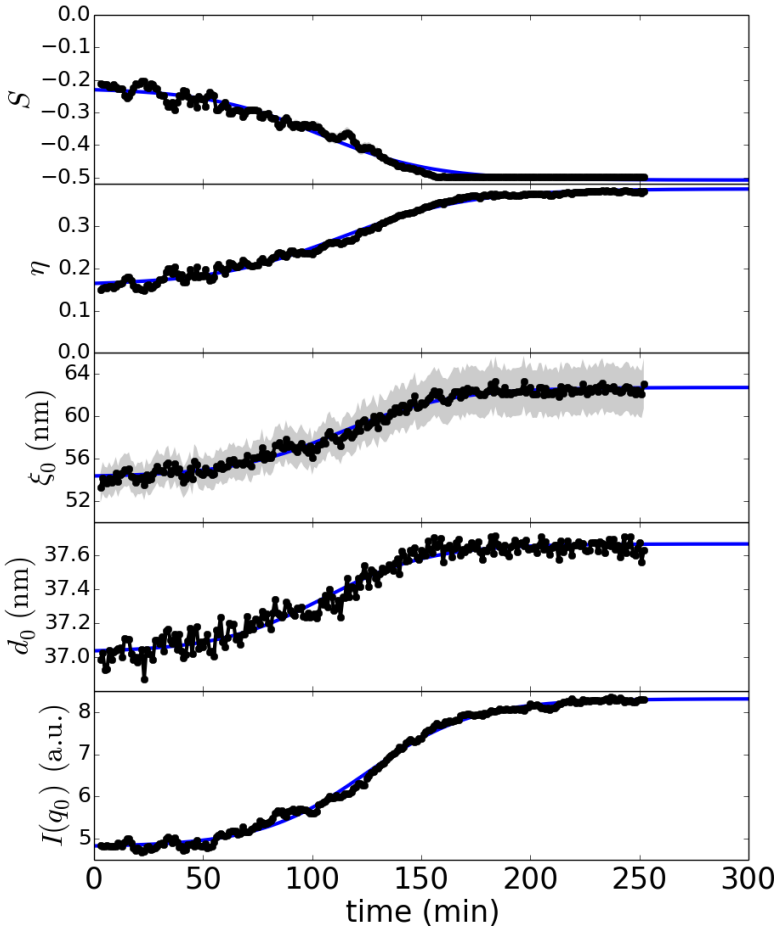

Figure 4. Kinetics of a concentrated CNC suspension (8.25 wt%) ordering within a magnetic field (1.2 T). Black dots are experimental data. The error bands are shown in light grey, estimated using the standard error of regression; these bands are typically smaller than the data points except in the case of the correlation length, ξ_0, in which the uncertainty in instrumental resolution dominates. Blue lines are fits to Equation 3 in the Experimental section. As ordering proceeds, inter-particle distances (d_0) and correlation lengths (ξ_0) increase. Measures of orientational order (η, S) also increase with time, as the magnetic field anti-aligns the CNCs.

Notably, the absolute values of measures of structural anisotropy (η, S) increase as a function of time within the magnetic field following a sigmoidal profile similar to I, d_0 and ξ_0 (Figure 4). This curve shape suggests that the magnetic-field induced reorientation is a cooperative process, coupling to the inherent CNC liquid crystalline ordering behavior, and occurs on a timescale of $\tau = 129 \pm 1$ min for 8.25 wt% CNC suspensions under a 1.2 T magnetic

field. (The variable τ represents the time required to achieve 73% alignment as described in the Experimental Section, and is calculated from the blue fits shown in Figure 4, according to Equation 3 also described in the Experimental Section.) The final value of the order parameter $S_f = -0.499$ suggests a nearly perfectly aligned system with CNCs oriented perpendicularly to the magnetic field (i.e. anti-aligned).

Figure 5 compares the ordering of CNC suspensions as a function of magnetic field strength. Decreasing the field strength from 1.2 T to 0.56 T increases the time required to align the concentrated 8.25 wt% suspension ($C > C^*$) by 36% ($\tau = 175 \pm 2$ min) but does not affect the ultimate degree of alignment, which still reaches $S_f = -0.499$. For both the 1.65 wt% suspension (Figure S3, Supporting Information, $C << C^*$) and the 4.13 wt% suspension ($C < C^*$) in the strongest magnetic field (1.2 T), the order parameter is essentially zero over the entire test period ($S_f = -0.02$, not statistically different from 0), confirming that the ordering of dilute suspensions of CNCs derived from cotton or wood pulp is not possible within the magnetic field strengths studied. This suggests that the magnetic forces on individual CNCs are not sufficient to yield aligned phases, and that cooperative ordering is required. Moreover, the lack of field-induced alignment even at concentrations where local organization (particle-particle interactions) is observed (Figure 2), suggests that the presence of simple particle-particle interactions in suspension prior to the formation of a macroscopic liquid crystalline phase, is not sufficient for cooperative ordering.

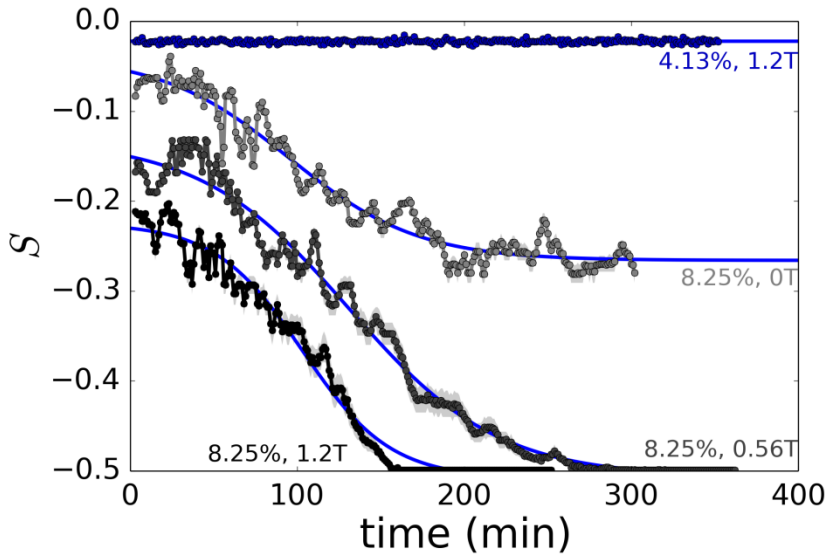

Figure 5. Time-evolution of the orientation order parameter (S) for CNC suspensions subjected to a magnetic field. The low-concentration system does not appreciably orient in response to the applied field. The high concentration suspensions exhibit strong orientation, with orientation kinetics influenced by the applied field strength.

In comparison, the concentrated 8.25 wt% suspension outside of the magnetic field exhibits anisotropy, evolving sigmoidally from $S_i = -0.04 \pm 0.01$ to an apparent plateau at $S_f = -0.26 \pm 0.01$ over a timescale of $\tau = 134 \pm 4$ min, again indicative of cooperative ordering, as expected at $C > C^*$. (Timescale-to-align values as a function of magnetic field strength are plotted in the Supporting Information, Figure S4, however, they are not directly comparable because the S_f values are different inside and out of the magnetic field.) This non-zero S value suggests the presence of large grains (or tactoids) of ordered material[48,49] (on the order of the beam size, ~ 300 μm). CNC tactoids have been shown to reach many hundreds of micrometers in diameter even for a 3 wt% CNC suspension,[5] and so the combination of working at higher concentrations and the potential directional coarsening over time due to the capillary sidewalls implies that the partial alignment detected by SAXS for the sample outside of a magnetic field is reasonable.

Somewhat surprisingly, the concentrated CNC suspensions ($C > C^*$) in a magnetic field are already significantly aligned (and significantly more so than samples not exposed to a magnetic field) even at the earliest time point measured (Figure 5). For example, an 8.25 wt% suspension in a 1.2 T magnetic field achieved $S_i = -0.22 \pm 0.01$ within the first 2 min, only slightly less than the final order parameter achieved outside a magnetic field for the same CNC suspension after 300 min. This suggests that the magnetic field provides an initial push to encourage fast formation of chiral nematic tactoids, followed by a slower cooperative "cleaning-up" of the chiral nematic structure to give a uniform liquid crystal texture across the sample whereby CNCs are all perpendicular to the magnetic field. This result was corroborated with polarized optical microscopy, showing the progression of chiral nematic tactoid coarsening in an 8.25 wt% CNC suspension exposed to a 0.56 T magnetic field (Figure 6).

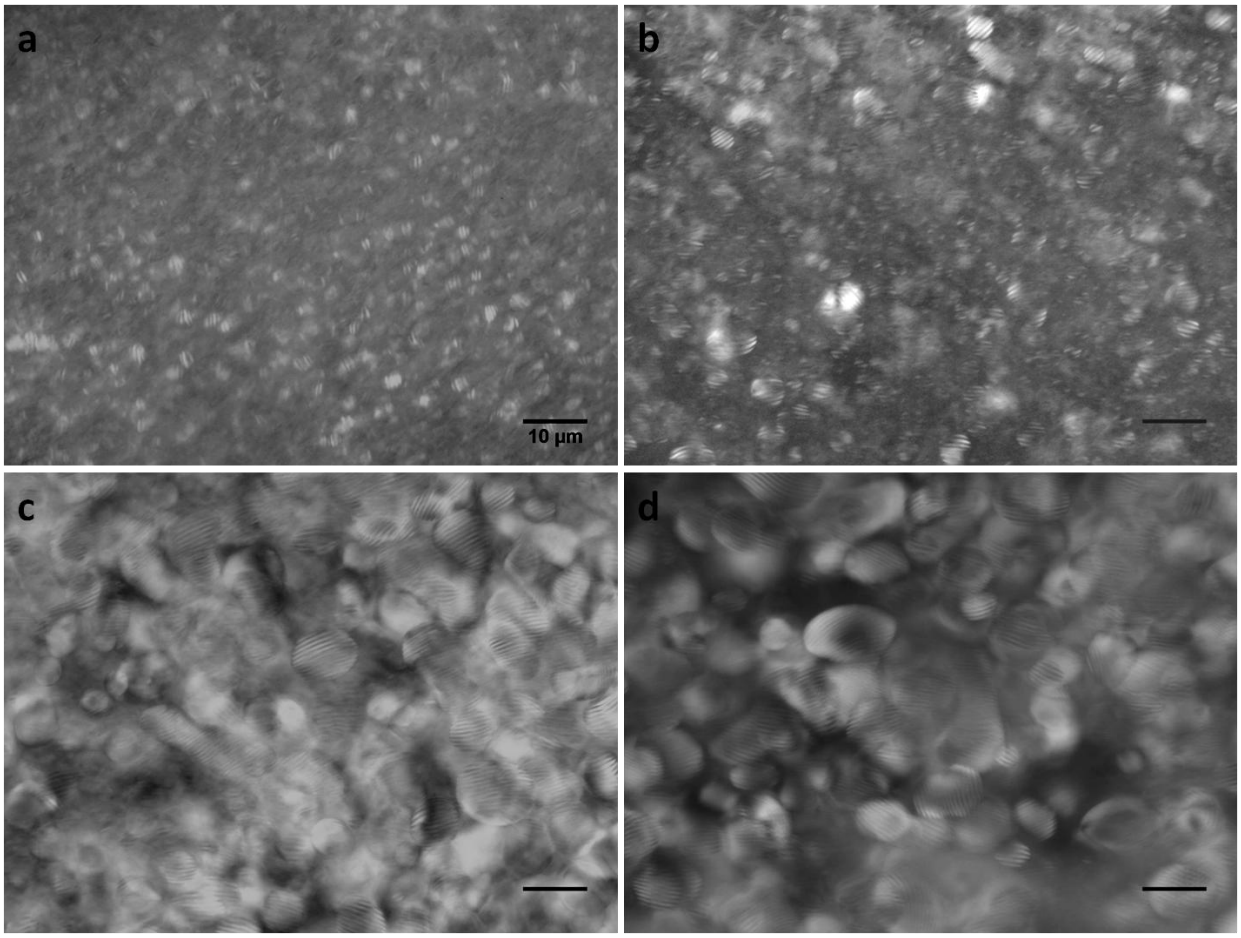

Figure 6. Polarized optical micrographs of an 8.25 wt% CNC suspension (a) directly after filling in a flat capillary, and upon exposure to a 0.56 T magnetic field for (b) 5 minutes, (c) 1 hour, and (d) 5 hours. The chiral nematic tactoids are present initially, grow rapidly upon exposure to the magnetic field, and further coarsen within the field over time. The chiral nematic pitch can be measured from the characteristic "fingerprint" texture and is constant at constant CNC concentration. All scale bars are 10 µm.

This result is significant for practical processing of CNCs, as rapid initial ordering of perturbed (disordered) suspensions may be desired, and a few minutes in a relatively weak magnetic field may produce a sufficient degree of CNC alignment depending on the desired application. Note that while some degree of ordering may be associated with shear alignment of CNCs during capillary filling,[19,50] or capillary sidewall-induced alignment, the deliberate focusing of the SAXS x-ray beam on the central ~300 um of the ~800 um diameter capillary and

the significantly lower amount of order detected in the 0 T experiment clearly indicates that the most significant driving force for alignment is the applied magnetic field.

It is challenging to directly compare the results presented here to the literature for a number of reasons. First, our results are for cotton-derived CNCs while most of the other magnetic alignment studies have used tunicate-derived CNCs which have a much lower C^* (0.85 wt%[51]) due to their higher aspect ratio. Tunicin CNCs are also slightly more crystalline than CNCs extracted from plant cellulose,[52] and may have a different surface charge density thus the diamagnetic susceptibility of each type of CNC will vary. Second, previous experiments involved samples in a magnetic field for long times without intermediate time measurements, or allowed an open suspension of CNCs to dry completely such that the aligned films can be analyzed.[26] These techniques do not allow for the observation of short-term alignment or the kinetics of the ordering process, which can result in application of a field for unnecessarily long times. Third, the methods to characterize order vary significantly between different magnetic alignment studies (i.e. microscopy,[23,30] diffraction,[26,37,38] scattering,[28] rheology,[36] birefringence,[20,27,33] raman spectroscopy,[23] and circular dichroism[30–32]), few of which included a quantitative order parameter,[36,38] and most of which were not performed *in situ* in a magnetic field. Fourth, the magnetic field strength used in different studies is highly variable and uniformly higher than the fields studied herein; for wood and cotton CNCs above C^*, various experiments have shown alignment over 2-4 h or unspecified long times during suspension evaporation while inside 2.4 T,[28] 7 T,[24,31] 8 T[38] and 11.7 T[35] electromagnets. As such, while extracting trends from the past work is difficult, this current work uniquely presents the evolution of the order parameters as a function of time (showing surprisingly fast ordering at

very short timescales) and demonstrates the most "mild" alignment conditions reported to date: near-perfect alignment in < 200 min in a 0.56 T rare earth magnet for cotton CNCs above *C**.

For the samples below *C** tested here, no improvement in order is detectable at field strengths of 0.56–1.2 T, despite previous research which shows uniaxial alignment of CNCs from tunicates below *C**.[26,27] Cotton-Mouton experiments by Frka-Petesic *et al*.[27] demonstrated a plateau in the optical birefringence of dilute tunicin CNC samples while sweeping the field strength up to 17.5 T and back to 0 T over 30 min, although full alignment was only observed with the strongest field. The lowest field strength used for dilute tunicin CNC alignment previous to that was 7 T[26]; however, alignment was only observed after evaporation, effectively concentrating the CNC suspension beyond *C**. To the best of our knowledge, ordering of dilute suspensions of plant-derived CNCs in a magnetic field without subsequent evaporation has never been demonstrated. Cooperative ordering in a magnet, and lack thereof for cotton CNCs below *C**, was also concluded by Tatsumi *et al.* who showed that the anisotropic phase of cotton CNCs led to their alignment within composites whereas the isotropic phase led to no such orientation under a 8 T field.[38] In our case, we believe that the detection of alignment was not feasible for the 4.13 and 1.65 wt% suspensions due to the relatively weak field strengths screened herein and the fast relaxation due to Brownian motion of particles in dilute suspension. As such, either much stronger fields, higher aspect ratio CNCs or more viscous suspensions are likely required for such alignment. Practically, this implies that it would not be industrially feasible to produce magnetically aligned systems from dilute suspensions of CNCs. We note that the phase diagram of the liquid crystalline behavior of CNCs shifts when polymers are grafted,[29] or when polymers that adsorb[53] or do not adsorb[54,55] to cellulose are combined with CNCs in suspension, thereby reducing *C** substantially. As such we predict that cooperative magnetic alignment of CNC

composite materials containing other polymers, surfactants and additives can be achieved at lower overall CNC contents in relatively weak magnetic fields.

Conclusions

In conclusion, we have demonstrated the capacity to achieve near-perfect anti-aligned chiral nematic suspensions of CNCs at relatively low magnetic field strengths over short timescales (<200 min). This ordering occurs in two stages, with an initial partial alignment occurring within minutes followed by slower subsequent coarsening (reorientation of chiral nematic tactoids) indicative of a cooperative process, as demonstrated through both SAXS and POM observations. The alignment is faster at higher field strengths (τ = 175 min for 0.56 T, τ = 129 min for 1.2 T). Dilute suspensions of CNCs did not order appreciably over time when exposed to an external magnetic field, suggesting that the propensity of CNCs to order into chiral nematic textures is a pre-requisite for magnetic alignment under these conditions. We anticipate that these results – in particular the success of alignment under relatively weak magnetic fields, and the observation of fast initial ordering in response to increasing magnetic field strengths – will be highly relevant to the design and fabrication of aligned nanocomposites with enhanced mechanical performance, liquid crystals and dried CNC films with controlled optical properties, model surfaces for the study of fundamental cellulose-cellulose and cellulose-polymer interactions, and templates and scaffolds with controlled directionality (e.g. for tissue engineering).

Supporting Information. Polarized optical micrographs for different concentration CNC suspensions, modeling details of CNC alignment in a magnetic field as seen by small angle x-ray scattering, and calculation of order parameters. This material is available free of charge via the Internet at http://pubs.acs.org.

Corresponding Author

*E-mail: ecranst@mcmaster.ca

Author Contributions

The manuscript was written through contributions of all authors. All authors have given approval to the final version of the manuscript.

Funding Sources

Funding from the Natural Sciences and Engineering Research Council of Canada (Discovery Grants RGPIN 356609 and 402329) as well as NSERC CREATE-IDEM (Integrated Design of Extracellular Matrices, grant 398058) is gratefully acknowledged.

Acknowledgements

We thank Yugang Zhang and Dmytro Nykypanchuk for assistance with the *in situ* magnetic cell, and Professor Jose Moran-Mirabal for assistance with polarized optical microscopy experiments. This research used resources of the Center for Functional Nanomaterials, which is a U.S. DOE Office of Science Facility, at Brookhaven National Laboratory under Contract No. DE-SC0012704.

References

(1) Habibi, Y.; Lucia, L. A.; Rojas, O. J. Cellulose Nanocrystals: Chemistry, Self-Assembly, and Applications. *Chem. Rev.* **2010**, *110* (6), 3479–3500.

(2) Future Markets Inc. *The Global Market For Nanocellulose to 2020*; 2013.

(3) Leung, A. C. W.; Hrapovic, S.; Lam, E.; Liu, Y.; Male, K. B.; Mahmoud, K. A.; Luong, J. H. T. Characteristics and Properties of Carboxylated Cellulose Nanocrystals Prepared

from a Novel One-Step Procedure. *Small* **2011**, *7* (3), 302–305.

(4) Rånby, B. G. Aqueous Colloidal Solutions of Cellulose Micelles. *Acta Chem. Scand.* **1949**, *3* (5), 649–650.

(5) Revol, J. F.; Bradford, H.; Giasson, J.; Marchessault, R. H.; Gray, D. G. Helicoidal Self-Ordering of Cellulose Microfibrils in Aqueous Suspension. *Int. J. Biol. Macromol.* **1992**, *14* (3), 170–172.

(6) Onsager, L. The Effects of Shape on the Interaction of Colloidal Particles. *Ann. N. Y. Acad. Sci.* **1949**, *51* (4), 627–659.

(7) Ureña-Benavides, E. E.; Ao, G.; Davis, V. A.; Kitchens, C. L. Rheology and Phase Behavior of Lyotropic Cellulose Nanocrystal Suspensions. *Macromolecules* **2011**, *44* (22), 8990–8998.

(8) Lagerwall, J. P. F.; Schütz, C.; Salajkova, M.; Noh, J.; Park, J. H.; Scalia, G.; Bergström, L. Cellulose Nanocrystal-Based Materials: From Liquid Crystal Self-Assembly and Glass Formation to Multifunctional Thin Films. *NPG Asia Mater.* **2014**, *6* (1), 1–12.

(9) Lin, N.; Huang, J.; Dufresne, A. Preparation, Properties and Applications of Polysaccharide Nanocrystals in Advanced Functional Nanomaterials: A Review. *Nanoscale* **2012**, *4* (11), 3274–3294.

(10) Giese, M.; Blusch, L. K.; Khan, M. K.; MacLachlan, M. J. Functional Materials from Cellulose-Derived Liquid-Crystal Templates. *Angew. Chemie Int. Ed.* **2015**, *54* (10), 2888–2910.

(11) Revol, J. F.; Godbout, L.; Gray, D. G. Solid Self-Assembled Films of Cellulose with Chiral Nematic Order and Optically Variable Properties. *J. Pulp Pap. Sci.* **1998**, *24* (5), 146–149.

(12) Bardet, R.; Belgacem, N.; Bras, J. Flexibility and Color Monitoring of Cellulose Nanocrystal Iridescent Solid Films Using Anionic or Neutral Polymers. *ACS Appl. Mater. Interfaces* **2015**, *7* (7), 4010–4018.

(13) Beck, S.; Bouchard, J.; Berry, R. Controlling the Reflection Wavelength of Iridescent Solid Films of Nanocrystalline Cellulose. *Biomacromolecules* **2011**, *12* (1), 167–172.

(14) Schlesinger, M.; Giese, M.; Blusch, L. K.; Hamad, W. Y.; MacLachlan, M. J. Chiral Nematic Cellulose-Gold Nanoparticle Composites from Mesoporous Photonic Cellulose. *Chem. Commun. (Camb).* **2015**, *51* (3), 530–533.

(15) Xu, J.; Nguyen, T.-D.; Xie, K.; Hamad, W. Y.; MacLachlan, M. J. Chiral Nematic Porous Germania and Germanium/carbon Films. *Nanoscale* **2015**, *7* (31), 13215–13223.

(16) Munier, P.; Gordeyeva, K.; Bergström, L.; Fall, A. B. Directional Freezing of Nanocellulose Dispersions Aligns the Rod-like Particles and Produces Low-Density and Robust Particle Networks. *Biomacromolecules* **2016**, *17*, 1875–1881.

(17) Dugan, J. M.; Collins, R. F.; Gough, J. E.; Eichhorn, S. J. Oriented Surfaces of Adsorbed Cellulose Nanowhiskers Promote Skeletal Muscle Myogenesis. *Acta Biomater.* **2013**, *9* (1), 4707–4715.

(18) Camarero-Espinosa, S.; Rothen-Rutishauser, B.; Weder, C.; Foster, E. J. Directed Cell Growth in Multi-Zonal Scaffolds for Cartilage Tissue Engineering. *Biomaterials* **2016**, *74*, 42–52.

(19) Abitbol, T.; Cranston, E. D. *Chapter 6: Directed Assembly of Oriented Cellulose Nanocrystal Films*; Oksman, K., Mathew, A. P., Bismarck, A., Rojas, O., Sain, M., Eds.; World Scientific, 2012.

(20) Frka-Petesic, B.; Jean, B.; Heux, L. First Experimental Evidence of a Giant Permanent

Electric-Dipole Moment in Cellulose Nanocrystals. *Europhys. Lett.* **2014**, *107* (2), 28006.

(21) Habibi, Y.; Heim, T.; Douillard, R. AC Electric Field-Assisted Assembly and Alignment of Cellulose Nanocrystals. *J. Polym. Sci. Part B Polym. Phys.* **2008**, *46* (14), 1430–1436.

(22) Kaddami, H.; Raihane, M. Electric Field Alignment of Nano Fibrillated Cellulose (NFC) in Silicone Oil: Impact on Electrical Properties. *ACS Appl. Mater. Interfaces* **2014**, *6* (12), 9418–9425.

(23) Pullawan, T.; Wilkinson, A. N.; Eichhorn, S. J. Influence of Magnetic Field Alignment of Cellulose Whiskers on the Mechanics of All-Cellulose Nanocomposites. *Biomacromolecules* **2012**, *13* (8), 2528–2536.

(24) Revol, J.-F.; Godbout, L.; Dong, X.-M.; Gray, D. G.; Chanzy, H.; Maret, G. Chiral Nematic Suspensions of Cellulose Crystallites; Phase Separation and Magnetic Field Orientation. *Liq. Cryst.* **1994**, *16* (1), 127–134.

(25) Hu, L.; Zhang, R.; Chen, Q. Synthesis and Assembly of Nanomaterials under Magnetic Fields. *Nanoscale* **2014**, *6* (23), 14064–14105.

(26) Sugiyama, J.; Chanzy, H.; Maret, G. Orientation of Cellulose Microcrystals by Strong Magnetic Fields. *Macromolecules* **1992**, *25* (16), 4232–4234.

(27) Frka-Petesic, B.; Sugiyama, J.; Kimura, S.; Chanzy, H.; Maret, G. Negative Diamagnetic Anisotropy and Birefringence of Cellulose Nanocrystals. *Macromolecules* **2015**, *48* (24), 8844–8857.

(28) Orts, W.; Godbout, L.; Marchessault, R. H.; Revol, J. F. Enhanced Ordering of Liquid Crystalline Suspensions of Cellulose Microfibrils: A Small Angle Neutron Scattering Study. *Macromolecules* **1998**, *31* (17), 5717–5725.

(29) Azzam, F.; Heux, L.; Jean, B. Adjustment Of The Chiral Nematic Phase Properties Of

Cellulose Nanocrystals By Polymer Grafting. *Langmuir* **2016**, acs.langmuir.6b00690.

(30) Dong, X. M.; Gray, D. G. Induced Circular Dichroism of Isotropic and Magnetically-Oriented Chiral Nematic Suspensions of Cellulose Crystallites. *Langmuir* **1997**, *13* (11), 3029–3034.

(31) Edgar, C. D.; Gray, D. G. Induced Circular Dichroism of Chiral Nematic Cellulose Films. *Cellulose* **2001**, *8* (1), 5–12.

(32) Pan, J.; Hamad, W.; Straus, S. K. Parameters Affecting the Chiral Nematic Phase of Nanocrystalline Cellulose Films. *Macromolecules* **2010**, *43* (8), 3851–3858.

(33) Kimura, F.; Kimura, T.; Tamura, M.; Hirai, A.; Ikuno, M.; Horii, F. Magnetic Alignment of the Chiral Nematic Phase of a Cellulose Microfibril Suspension. *Langmuir* **2005**, *21* (5), 2034–2037.

(34) Denisov, A. Y.; Kloser, E.; Gray, D. G.; Mittermaier, A. K. Protein Alignment Using Cellulose Nanocrystals: Practical Considerations and Range of Application. *J. Biomol. NMR* **2010**, *47* (3), 195–204.

(35) Fleming, K.; Gray, D. G.; Prasannan, S.; Matthews, S. Cellulose Crystallites: A New and Robust Liquid Crystalline Medium for the Measurement of Residual Dipolar Couplings. *J. Am. Chem. Soc.* **2000**, *122* (10), 5224–5225.

(36) Kim, D.; Song, Y. Rheological Behavior of Cellulose Nanowhisker Suspension under Magnetic Field. *Carbohydr. Polym.* **2015**.

(37) Song, G.; Kimura, F.; Kimura, T.; Piao, G. Orientational Distribution of Cellulose Nanocrystals in a Cellulose Whisker As Studied by Diamagnetic Anisotropy. *Macromolecules* **2013**, *46* (22), 8957–8963.

(38) Tatsumi, M.; Kimura, F.; Kimura, T.; Teramoto, Y.; Nishio, Y. Anisotropic Polymer

Composites Synthesized by Immobilizing Cellulose Nanocrystal Suspensions Specifically Oriented under Magnetic Fields. *Biomacromolecules* **2014**, *15* (12), 4579–4589.

(39) Beck-Candanedo, S.; Roman, M.; Gray, D. G. Effect of Reaction Conditions on the Properties and Behavior of Wood Cellulose Nanocrystal Suspensions. *Biomacromolecules* **2005**, *6* (2), 1048–1054.

(40) Beck, S.; Méthot, M.; Bouchard, J.; Me, M.; Bouchard, J. General Procedure for Determining Cellulose Nanocrystal Sulfate Half-Ester Content by Conductometric Titration. *Cellulose* **2015**, 101–116.

(41) Ruland, W.; Tompa, H. The Effect of Preferred Orientation on the Intensity Distribution of (Hk) Interferences. *Acta Crystallogr. Sect. A* **1968**, *24* (1), 93–99.

(42) Ruland, W.; Smarsly, B. SAXS of Self-Assembled Oriented Lamellar Nanocomposite Films: An Advanced Method of Evaluation. *J. Appl. Crystallogr.* **2004**, *37* (4), 575–584.

(43) Yager, K. G.; Forrey, C.; Singh, G.; Satija, S. K.; Page, K. A.; Patton, D. L.; Douglas, J. F.; Jones, R. L.; Karim, A. Thermally-Induced Transition of Lamellae Orientation in Block-Copolymer Films on "neutral" Nanoparticle-Coated Substrates. *Soft Matter* **2015**, *11*, 5154–5167.

(44) Majewski, P. W.; Osuji, C. O. Non-Degenerate Magnetic Alignment of Self-Assembled Mesophases. *Soft Matter* **2009**, *5* (18), 3417.

(45) Uhlig, M.; Fall, A.; Wellert, S.; Lehmann, M.; Prévost, S.; Wågberg, L.; von Klitzing, R.; Nyström, G. Two-Dimensional Aggregation and Semidilute Ordering in Cellulose Nanocrystals. *Langmuir* **2016**, *32* (2), 442–450.

(46) Schütz, C.; Agthe, M.; Fall, A. B.; Gordeyeva, K.; Guccini, V.; Salajková, M.; Plivelic, T. S.; Lagerwall, J. P. F.; Salazar-Alvarez, G.; Bergström, L. Rod Packing in Chiral Nematic

Cellulose Nanocrystal Dispersions Studied by Small-Angle X-Ray Scattering and Laser Diffraction. *Langmuir* **2015**, *31*, 6507–6513.

(47) Beck-Candanedo, S.; Viet, D.; Gray, D. G. Triphase Equilibria in Cellulose Nanocrystal Suspensions Containing Neutral and Charged Macromolecules. *Macromolecules* **2007**, *40* (9), 3429–3436.

(48) Choi, K.-J.; Spruiell, J. E.; White, J. L. Orientation and Morphology of High-Density Polyethylene Film Produced by the Tubular Blowing Method and Its Relationship to Process Conditions. *J. Polym. Sci. Polym. Phys. Ed.* **1982**, *20* (1), 27–47.

(49) Ghosh, S. K. A Model for the Orientational Order in Liquid Crystals. *Nuovo Cim. D* **1984**, *4* (3), 229–244.

(50) Ebeling, T.; Paillet, M.; Borsali, R.; Diat, O.; Dufresne, A.; Cavaillé, J. Y.; Chanzy, H. Shear-Induced Orientation Phenomena in Suspensions of Cellulose Microcrystals, Revealed by Small Angle X-Ray Scattering. *Langmuir* **1999**, *15* (19), 6123–6126.

(51) Bercea, M.; Navard, P. Shear Dynamics of Aqueous Suspensions of Cellulose Whiskers. *Macromolecules* **2000**, *33* (16), 6011–6016.

(52) Moon, R. J.; Martini, A.; Nairn, J.; Simonsen, J.; Youngblood, J. Cellulose Nanomaterials Review: Structure, Properties and Nanocomposites. *Chem. Soc. Rev.* **2011**, *40* (7), 3941–3994.

(53) Hu, Z.; Cranston, E. D.; Ng, R.; Pelton, R. Tuning Cellulose Nanocrystal Gelation with Polysaccharides and Surfactants. *Langmuir* **2014**, *30* (10), 2684–2692.

(54) Edgar, C. D.; Gray, D. G. Influence of Dextran on the Phase Behavior of Suspensions of Cellulose Nanocrystals. *Macromolecules* **2002**, *35* (19), 7400–7406.

(55) Beck-Candanedo, S.; Viet, D.; Gray, D. G. Induced Phase Separation in Cellulose

Nanocrystal Suspensions Containing Ionic Dye Species. *Cellulose* **2006**, *13*, 629–635.

Table of Contents Graphic.